Direct Observation of OH Radicals Ejected from Water Ice Surface in the Photoirradiation of Nitrate Adsorbed on Ice at 100 K

Akihiro Yabushita, Daisuke Iida, Tetsuya Hama, and Masahiro Kawasaki*

Department of Molecular Engineering, Kyoto University, Kyoto 615-8510, Japan

Received: May 26, 2008; Revised Manuscript Received: July 13, 2008

Production of gaseous OH radicals in the 248−350 nm photoirradiation of NO_3^- doped on amorphous ice at 100 K was monitored directly by using resonance-enhanced multiphoton ionization. The translational energy distribution of the OH product was represented by a Maxwell−Boltzmann energy distribution with the translational temperature of 3250 ± 250 K. The rotational temperature was estimated to be 175 ± 25 K. We have confirmed that the OH production should be attributed to the secondary photolysis of H_2O_2 produced on ice surface on the basis of the results of controlled photolysis experiments for H_2O_2 doped on ice surface.

Introduction

Photochemical reactions transpiring in bulk ice and at the ice surface are known to be important processes in polar and alpine snowpack chemistry.[1] Because of ubiquity and high water solubility, nitric acid (HNO_3) is a common trace compound in most snow samples even in remote polar regions. Therefore, photochemical reactions in aqueous solutions and bulk ice pellets have been extensively investigated.[2−9] Nitrate (NO_3^-) plays a crucial role in snowpack oxidation chemistry, acting as a photolytic source of hydroxyl radicals, OH.[10] The summertime atmospheric boundary layer over the South Pole is observed to be strongly oxidizing with unexpectedly high levels of OH.[11,12]

An ultraviolet irradiation of an aqueous solution of nitric acid, a strong oxidant, generates oxygen atoms and O^- anions that readily react with H^+ to form OH under most environmental conditions. The secondary photolysis of HONO products is also a source of OH. The energetics of the OH production processes after the ultraviolet photolysis of nitrate in an aqueous solution is listed;[13,14]

	ΔH/ kJ mol^{-1}	λ_{th}/nm	
$NO_3^-(d) + h\nu \rightarrow O(^3P)(g) + NO_2^-(d)$	352	340	(1)
$NO_3^-(d) + h\nu \rightarrow O^-(d) + NO_2(g)$	190	629	(2)
$NO_2^-(d) + H_2O(l) \rightarrow HONO(d) + OH^-(d)$	41	-	(3)
$NO_2^-(d) + h\nu \rightarrow O^-(d) + NO(g)$	145	827	(4)
$O^-(d) + H^+(aq)/H_3O^+(aq) \rightarrow OH(g)(+H_2O(aq))$	−323	-	(5)
$HONO(d) + h\nu \rightarrow OH(g) + NO(g)$	248	482	(6)

where λ_{th} stands for the threshold wavelength, d stands for dilute aqueous solution, g stands for gas phase, and aq stands for aqueous solution. Previous laboratory studies concerning the photolysis of NO_3^- on/in water ice employed resonance-enhanced multiphoton ionization (REMPI) detection for $O(^3P_2)$ atom and NO molecule,[15] laser-induced fluorescence detection for NO_2,[4,5] or product analysis of reactions with a radical scavenger in the aqueous solution.[6,7] OH radicals in the photoirradiation of NO_3^- were measured by using benzoic acid (BA) as a chemical probe where OH reacts with BA to form *p*-HBA.[9] However, the scavenger techniques are only able to detect OH remaining on/in the ice and in the aqueous solution. Direct release of OH from the ice surface during the ultraviolet photoirradiation of NO_3^- has not been previously observed. If OH radicals are produced under condensed phase, they recombine to form H_2O_2 under low-temperature ice conditions. The main source of OH in the gas phase of the polar region has been considered to be the UV photolysis of H_2O_2 that deposits on snow from the atmosphere.[16]

$$OH(d) + OH(d) \rightarrow H_2O_2(d) \quad (7)$$

$$H_2O_2(d) + h\nu \rightarrow 2OH(g) \quad (8)$$

In this work, we have focused on direct detection of OH produced from the ultraviolet photoirradiation of NO_3^- doped on a water ice film by using laser ionization time-of-flight (TOF) techniques to elucidate the reaction mechanisms on formation of gaseous OH from water ice.

Experimental Section

Photodissociation of nitrate and hydrogen peroxide doped on ice films at 100 K was carried out under a high-vacuum chamber, which was equipped with two turbo molecular pumps in tandem, a pulsed molecular beam, an excimer laser, and a dye laser. The experimental details are described elsewhere.[17] In brief, a vacuum chamber was evacuated to a base pressure of 10^{-8} Torr (Shimadzu, 800 and 50 Ls^{-1}). An optically flat sapphire substrate, sputter coated with a thin film of Au, was supported in the center of the chamber by a liquid-nitrogen-cooled manipulator connected to an X-Y-Z stage.[18] The temperature of the substrate was controlled to within 1 K with resistive heating. Amorphous solid water (ASW) films were prepared with the backfilling deposition of water vapor onto the substrate at 100 K for 60 min by a pulsed nozzle (General Valve) at a rate of 10 Hz at 20 Torr stagnation pressure of water

* Corresponding author. E-mail: kawasaki@photon.mbox.media.kyoto-u.ac.jp. Fax: +81-75-383-2573.

10.1021/jp804622z CCC: $40.75 © 2008 American Chemical Society
Published on Web 09/09/2008

vapor. The exposure was typically 1800 L (1 L = 1×10^{-6} Torr s) of gaseous water, which resulted in the formation of 600 monolayers of H_2O on the Au substrate.[19]

Commercially available nitric acid (69%) was dried in a glass container with concentrated sulfuric acid (97%) to remove water. The gas mixture of HNO_3 (30 Torr) with N_2 diluent (730 Torr) was introduced into a vacuum chamber by using the backfilling method by a pulsed nozzle. A sticking (uptake) coefficient of HNO_3 on ice is reported to be 0.3 at 197 K.[20] The exposure of HNO_3 to the ASW film was typically 1 L for 80 s duration at 100 K, and then, the substrate temperature was held at 130 K for up to 90 min to allow ionization to $H^+ + NO_3^-$. After the substrate temperature was reduced to 100 K, UV irradiation of the doped ice surface and REMPI detection of OH were performed.

For photolysis of H_2O_2 doped on ice surface commercially available H_2O_2 (30% aqueous solution) was concentrated in a glass container by vacuum distillation. The exposure of the H_2O_2/H_2O mixture vapor on the ASW film at 90 K was <10 L for 330 s duration. UV photoirradiation and REMPI detection of OH were performed at 90 K.

The ice film thus dosed was photodissociated at 248−350 nm with a YAG pumped dye laser and a KrF excimer laser (Lambda Physik, SCANmate and COMPex, 1 mJ cm^{-2} $pulse^{-1}$). Another YAG pumped dye laser was used to ionize the photofragments by the (2 + 1) REMPI transition of $OH(D^2\Sigma^- - X^2\Pi, 0-0)$ at 244.1−244.9 nm with a lens (f = 0.10 m). The subsequent REMPI signals were detected by a TOF mass spectrometer and normalized to the probe laser intensity. The distance, r, between the substrate and the detection region was varied from 2 to 5 mm to change the effective flight lengths for neutral OH photofragments, which was set typically to 2 mm. REMPI signal intensities were taken as a function of time delay, t, between the photolysis and probe laser pulses, which correspond to the flight time between the substrate and the REMPI detection region.

The TOF spectrum was fitted with a flux weighted Maxwell−Boltzmann (MB) distribution, $S(t,T_i)$, defined by the translational temperature T_i;

$$S_{MB}(t, r) = r^3 t^{-4} \exp[-mr^2/(2k_B T_{trans} t^2)] \quad (9)$$

$$P_{MB}(E_t) = (k_B T_{trans})^{-2} E_t \exp[-E_t/(k_B T_{trans})] \quad (10)$$

The MB distribution in energy frame, $P_{MB}(E_t)$, is characterized by the average translational energy, $\langle E_t \rangle = 2k_B T_{trans}$, where k_B is the Boltzmann constant and T_{trans} is the translational temperature.

Results

1. Resonance-Enhanced Multiphoton Ionization Detection of OH from the Photoirradiation to NO_3^- Doped on an ASW Film at 100 K. ***1.1. Excitation Spectrum and Temporal Evolution of OH Signal Intensity.*** Figure 1 shows the REMPI spectrum of $OH(D^2\Sigma^- - X^2\Pi, 0-0)$ from the 300 nm photoirradiation at 100 K. The delay between photolysis and probe laser pulse was t = 1.5 μs. By simulating the spectra, we estimated the rotational temperature to be $T_{rot} = 175 \pm 25$ K. The OH signal intensity dependence on the dissociation laser wavelength is shown in Figure 2, in which the aqueous absorption spectrum of H_2O_2 fits well, as shown by the solid curve.

Figure 3 shows the signal-intensity change of OH as a function of annealing time after deposition of HNO_3 on the ASW. Immediately after deposition of HNO_3 on ice, REMPI signal was not detected because the ionization of HNO_3 into H^+ and NO_3^- on a water ice film surface is a slow process. The rate constant for signal evolution is determined to be $k = (2.8 \pm 0.2) \times 10^{-3}$ s^{-1}, which is in fair agreement with $(5.3 \pm 0.2) \times 10^{-3}$ s^{-1} at 130 K of our previous experiments[15] and $(4.9 \pm 0.7) \times 10^{-3}$ s^{-1} of Pursell et al. who monitored ionization kinetics at 130−150 K by transmission FTIR spectroscopy.[21]

1.2. Translational Temperatures and Incident Laser Power Dependence of OH. Figure 4 shows a TOF spectrum of OH from the 300 nm photoirradiation of NO_3^- on ASW at 100 K. The TOF spectrum is well reproduced by a MB distribution with $T_{trans} = 3250 \pm 250$ K. As a function of laser intensity at

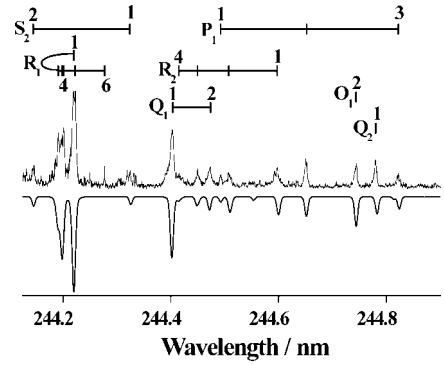

Figure 1. (top) REMPI excitation spectrum of OH(D−X, 0−0) from the 300 nm photoirradiation on the NO_3^- doped on an ASW film. (bottom) Simulated spectrum obtained by assuming a Boltzmann distribution with T_{rot} = 175 K. Ice temperature = 100 K and TOF = 1.5 μs. Q, R, and S stand for spectral assignments for rotational branches.

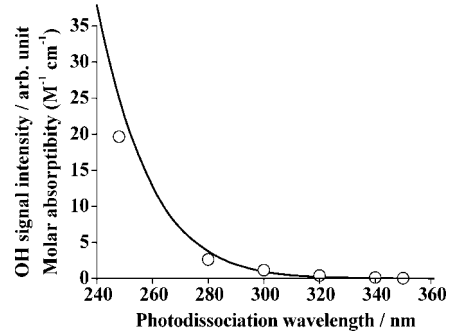

Figure 2. Photolysis wavelength dependence of OH signal intensity for the rotational level of R(1) + R(5) from the photoirradiation on the NO_3^- doped on an ASW film. Ice temperature = 100 K and TOF = 1.5 μs. The solid curve is the absorption spectrum of H_2O_2 in aqueous solution.[31]

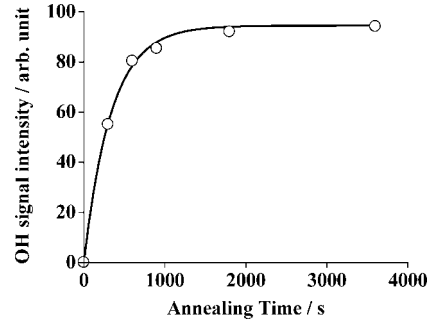

Figure 3. Annealing time evolution of OH signal intensity for the rotational level of R(1) + R(5) after deposition of HNO_3 on an ASW film. Ice temperature = 130 K and TOF = 1.5 μs. During the intercept of measurement, the UV photoirradiation beam at 300 nm was blocked. The measured evolution curve is fitted to a single exponential curve with a rate constant of 2.8×10^{-3} s^{-1}.

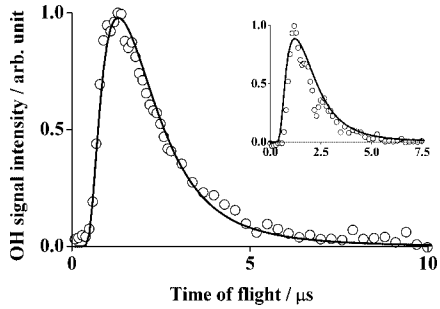

Figure 4. TOF spectrum of OH for the transition of R(1) + R(5) from the 300 nm photoirradiation of NO_3^- doped on an ASW film at 100 K. The solid curve is a fit to the data derived by assuming a MB distribution, $T_{trans} = 3250$ K. The inset shows OH from the 300 nm photodissociation of H_2O_2 doped on an ASW film and is represented with $T_{trans} = 3750$ K.

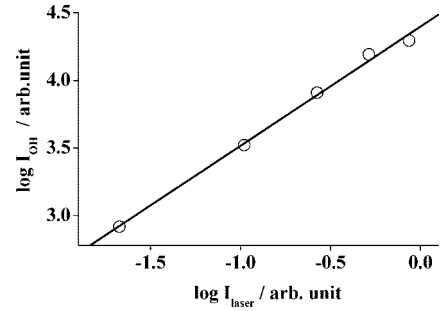

Figure 5. Incident laser power dependence of the OH signal intensity for the transition of R(1) + R(5) from the 300 nm photoirradiation of NO_3^- doped on an ASW film. Ice temperature = 100 K and $t = 1.5$ μs. The slope is 0.88.

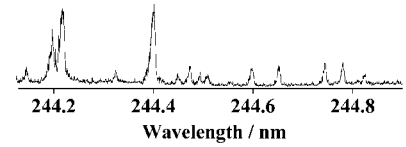

Figure 6. REMPI spectrum of OH from the 300 nm photodissociation of H_2O_2 on an ASW film. Ice temperature = 90 K and TOF = 1.5 μs. The spectrum is reproducedby assuming a Boltzmann distribution with $T_{rot} = 225$ K.

300 nm, the OH signal intensity was measured at $t = 1.5$ μs (the peak TOF time). The linear slope of the signal intensity dependence on the incident laser power dependence is 0.88 ± 0.03 as shown in Figure 5.

2. Photodissociation of H_2O_2 Doped on ASW at 100 K. As a control experiment, we performed the 300 nm photodissociation of H_2O_2 doped on ASW at 90 K. The TOF spectrum of OH in the inset of Figure 4 is reproduced with $T_{trans} = 3750$ ± 250 K. The incident laser power dependence on signal intensity was 0.72 ± 0.04. The REMPI spectrum of OH in Figure 6 was measured at $t = 1.5$ μs. The rotational temperature was estimated to be $T_{rot} = 225 \pm 25$ K. Without H_2O_2 adsorption on ice, no OH signals were detected in the 300 nm photoirradiation.

Discussion

1. Origin of OH from the UV Photoirradiation to Doped NO_3^- on Ice. The previously reported candidates for the formation mechanism of OH are ion recombination via nitrate photolysis and the secondary photolysis of HONO.[2]

$$O^-(d) + H^+(aq)/H_3O^+(aq) \rightarrow OH(g)(+H_2O(aq)) \quad (5)$$

$$HONO(d) + h\nu \rightarrow OH(g) + NO(g) \quad (6)$$

Figure 2 shows that the aqueous absorption spectrum of H_2O_2 increases monotonically with decreasing photolysis wavelength and fits well with the OH photoproduction curve, whereas those of NO_3^- and NO_2^- as well HONO[22] are totally different from the experimental results as shown in Figure 7. The relatively strong absorption spectrum of aqueous NO_2^- increases with wavelength and peaks at 355 nm.[23] Warneck and Wurzinger[7] reported the quantum yields at 305 nm for reactions 7 and 7 in aqueous solution to be 1.1×10^{-3} and 9.2×10^{-3}, respectively. Bartels-Rausch and Donaldson[24] reported the release of NO_2 and HONO during snowpack photochemistry. In an aqueous solution, the quantum yield for HONO production, $(3.8 \pm 0.6) \times 10^{-4}$, is approximately 1 order of magnitude lower than the quantum yield of NO_2.[24] Hence, we assume that the contribution of reaction 7 would be small also on ice surface. On the basis of the previously reported works,[1] reaction 7 could be another source for OH.

As described in Figures 2 and 7, on the basis of the facts that (a) the excitation spectrum fits well with the absorption spectrum of aqueous H_2O_2 and (b) the internal and kinetic energy distributions for both the NO_3^- and H_2O_2 photolysis are the same, most of OH would come from the photolysis of H_2O_2. The incident laser power dependence in Figure 5 suggests a one-photon process which is rationalized if the photolysis of H_2O_2, reaction 8, is a rate determination process for gaseous production of OH from ice surface.

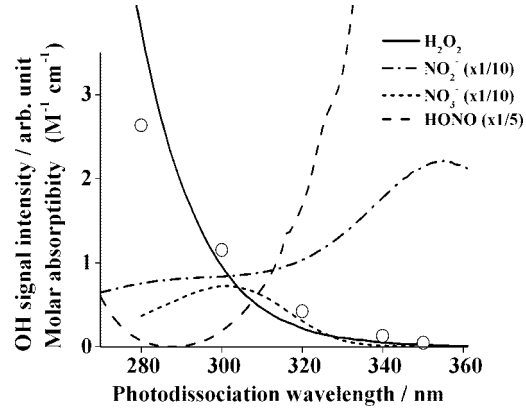

Figure 7. Photolysis wavelength dependence of OH signal intensity for the transition of R(1) + R(5) from the photoirradiation of NO_3^- doped on an ASW film. The solid curves are the absorption spectra of HONO, NO_2^-, NO_3^-, and H_2O_2 in aqueous solution.[9,22,23,31]

2. Photoreactions of H_2O_2 on Ice Surface. In our previous experiments, TOF spectra of the $O(^3P_2)$ atoms produced during the 305 nm photodissociation of NO_3^- on a polycrystalline ice film at 100 K consisted of fast and slow components.[15] The fast component derives from the photodissociation of NO_3^- doped on the ice surface via reaction 7. The slow component with $T_{trans} = 100$ K is attributed to O atoms which are accommodated to 100 K bulk ice. However, the TOF spectrum of the OH radical in Figure 4 consists of only one component with $T_{trans} = 3250 \pm 250$ K corresponding to 54 ± 4 kJ/mol, which comes from the photodissociation of H_2O_2 doped on the ice surface and not in the bulk phase. The lack of a slow TOF component of OH could be attributed to its high reactivity and strong H bonding of OH. If the OH produced initially collides with a cold surface, it will be strongly sorbed to the ice film and likely react with other chemical species present. Because the classical barrier height for the hydrogen abstraction in the gas phase, HO + $H_2O \rightarrow H_2O$ + OH, is 32.6 kJ/mol,[25] the

hydrogen abstraction reaction possibly occurs on/in ice surface. Molecular dynamic calculations were previously reported by using analytical potentials to simulate photodissociation of water in ice at 10 K.[26] These calculations show that upon photodissociation to H + OH, only 9% of the trajectories originating in the first layer lead to OH desorbing; that is, most of OH are trapped on/in ice. The uptake coefficient of OH on a fresh ice surface was 0.1. The uptake coefficient could be significantly increased by adsorbing HNO_3 to the surface or melting the ice surface.[27]

In the gas phase at room temperature, photodissociation of H_2O_2 at 248 nm yields OH radicals with $\langle E_{rot}\rangle = 13$ kJ mol^{-1} and $\langle E_{trans}\rangle = 269$ kJ mol^{-1} or the ratio $\langle E_{rot}\rangle/\langle E_{trans}\rangle = 0.048$.[28] The present experimental ratios for the NO_3^- and H_2O_2 photolysis, $\langle E_{rot}\rangle/\langle E_{trans}\rangle = k_BT_{rot}/2k_BT_{trans} = 0.027$ (= 175 K/(2 × 3250 K)) and 0.030 (= 225 K/(2 × 3750 K)) are in fair agreement with the gas-phase value, 0.048. This is because the center-of-mass position of OH is almost on the oxygen atom, and hence, rotational excitation is much lower than translational excitation, which are induced by the impulse upon departing of OH from surface. For photo- and electron-stimulated desorption dynamics, the translational energy distribution is determined by the lifetime on the excited potential and rotational energy distribution depends on the rotational−translational coupling.[29,30] Because the detailed nature of the potential energy surfaces for H_2O_2 on water ice is not presently available, we will not discuss the desorption dynamics qualitatively.

3. Atmospheric Implications. The present results show direct release of gaseous OH from the photoirradiation of NO_3^- doped on ice films at 100 K by using UV wavelengths of the solar spectrum present in the troposphere. The formation process of OH from the photodissociation reaction of H_2O_2 is proposed to be the secondary reaction. The following important question arises: does the present low-temperature photochemistry discussed above have a relevance to the snowpack observations? Our present results imply that OH departs directly from ice surface in the photodissociation of surface doped H_2O_2 molecule and not from H_2O_2 in the bulk phase. Because the excess energy in the UV photodissociation is large enough, the photoinduced processes would be independent of the surface temperature as far as H_2O_2 photodissociation concerns.

The photodissociation of H_2O_2 is interesting, because it could be one of the OH sources in some locations.[3,10,31] The present results might imply a direct photochemical production of OH for polar and alpine snowpack chemistry. Cirrus clouds in the upper troposphere also contain nitrate, the UV photodissociation of which could be a source of OH radicals via the H_2O_2 photolysis. Because HNO_3 adsorb readily to ice in polar regions and in high-altitude cirrus clouds,[31] the H_2O_2 photolysis could be a plausible pathway for the direct atmospheric production of gaseous OH.

Acknowledgment. The authors thank Mr. M. Yokoyama for his help with experiments and Prof. H.-P. Loock of Queen's University for discussion. This work is supported by a grant-in-aid from the Ministry of Education and Science, Japan.

References and Notes

(1) Grannas, A. M.; Jones, A. E.; Dibb, J.; Ammann, M.; Anastasio, C.; Beine, H J.; Bergin, M.; Bottenheim, J.; Boxe, C. S.; Carver, G. ; Chen, G. ; Crawford, J. H.; Domin'e, F.; Frey, M. M.; Guzm'an, M. I.; Heard, D. E.; Helmig, D.; Hoffmann, M. R.; Honrath, R. E.; Huey, L. G.; Hutterli, M.; Jacobi, H. W.; Kl'an, P.; Lefer, B.; McConnell, J.; Plane, J.; Sander, R.; Savarino, J.; Shepson, P. B.; Simpson, W. R.; Sodeau, J. R.; von Glasow, R.; Weller, R.; Wolff, E. W.; Zhu, T. *Atmos. Chem. Phys.* **2007**, *7*, 4329.

(2) Jacobi, H.-W.; Hilker, B. *J. Photochem. Photobiol. A* **2007**, *185*, 371.

(3) Jacobi, H.-W.; Annor, T.; Quansah, E. *J. Photochem. Photobiol. A* **2006**, *179*, 330.

(4) Dubowski, Y.; Colussi, A. J.; Hoffmann, M. R. *J. Phys. Chem. A* **2001**, *105*, 4928.

(5) Dubowski, Y.; Colussi, A. J.; Boxe, C.; Hoffmann, M. R. *J. Phys. Chem. A* **2002**, *106*, 6967.

(6) Mack, J.; Bolton, J. R. *J. Photochem. Photobiol. A* **1999**, *128*, 1.

(7) Warneck, P.; Wurzinger, C. *J. Phys. Chem.* **1988**, *92*, 6278.

(8) Mark, G.; Korth, H.-G.; Schuchmann, H.-P.; von Sonntag, C. *J. Photochem. Photobiol. A* **1996**, *101*, 89.

(9) Chu, L.; Anastasio, C. *J. Phys. Chem. A* **2003**, *107*, 9594.

(10) France, J. L.; Kinga, M. D.; Lee-Taylor, J. *Atmos. Environ.* **2007**, *41*, 5502.

(11) Jones, A. E.; Wolff, E. W. *J. Geophys. Res., [Atmos.]* **2003**, *108*, 4565.

(12) Mauldin, R. L.; Eisele, F. L.; Tanner, D. J.; Kosciuch, E.; Shetter, R.; Lefer, B.; Hall, S. R.; Nowack, J. B.; Buhr, M.; Chen, G.; Wang, P.; Davis, D. *Geophys. Res. Lett.* **2001**, *28*, 3629.

(13) Karapet'yants, M. Kh.; Karapet'yants, M. K. *Handbook of thermodynamic constants of inorganic and organic compounds*; Ann Arbor-Humphrey Science Publishers, 1970.ΔH in unit of kJmol^{-1}: O(^{3}P$_2$)(g) = 249.2, O$^-$(*d*) =−50.21, OH(g) = 39.0, OH$^-$(d) =−230.0, NO(g) = 90.2, H_2O(l) =−285.8, NO_2(g) = 33.18, NO_2^-(d) =−104.6, HONO(d) =−119.2, NO_3^-(d) =−207.4. We have adapted H^+(aq) = 412 kJ equiv^{-1} as the standard enthalpy change of formation for the reaction (1/2)H_2(g) → H^+(aq), which is calculated by Myers.[14]

(14) Myers, R. T. *Ohio. J. Sci.* **1968**, *68*, 123.

(15) Yabushita, A.; Kawanaka, N.; Kawasaki, M.; Hamer, P. D.; Shallcross, D. E. *J. Phys. Chem. A* **2007**, *111*, 8629.

(16) Legrand, M.; Mayewski, P. *Rev. Geophys.* **1997**, *35*, 219.

(17) Yabushita, A.; Inoue, Y.; Senga, T.; Kawasaki, M.; Sato, S. *J. Phys. Chem. B* **2002**, *106*, 3151.

(18) Kawasaki, M. *Appl. Surf. Sci.* **1998**, *135*, 115.

(19) Sato, S.; Yamaguchi, D.; Nakagawa, K.; Inoue, Y.; Yabushita, A.; Kawasaki, M. *Langmuir* **2000**, *16*, 9533.

(20) Leu, M.-T. *Geophys. Res. Lett.* **1998**, *15*, 17.

(21) Pursell, C. J.; Everest, M. A.; Falgout, M. A.; Sanchez, D. D. *J. Phys. Chem. A* **2002**, *106*, 7764.

(22) Riordan, E.; Minogue, N.; Healy, D.; O'Driscoll, P.; Sodeau, J. R. *J. Phys. Chem. A* **2005**, *109*, 779.

(23) Chu, L.; Anastasio, C. *Environ. Sci. Technol.* **2007**, *41*, 3626.

(24) Bartels-Rausch, T.; Donaldson, D. J. *Atmos. Chem. Phys. Discuss.* **2006**, *6*, 10713.

(25) Uchimaru, T.; Chandra, A. K.; Tsuzuki, S.; Sugie, M.; Sekiya, A. J. *Comput. Chem.* **2003**, *24*, 1538.

(26) Andersson, S.; Al-Halabi, A.; Kroes, G.-J.; van Dishoeck, E. F. *J. Chem. Phys.* **2006**, *124*, 064715.

(27) Cooper, P. L.; Abbatt, J. P. D. *J. Phys. Chem.* **1996**, *100*, 2249.

(28) Ondrey, G.; van Veen, N.; Bersohn, R. *J. Chem. Phys.* **1983**, *78*, 3732.

(29) Menzel, D.; Gomer, R. *J. Chem. Phys.* **1964**, *41*, 3311.

(30) Redhead, P. A. *Can. J. Phys.* **1964**, *42*, 886.

(31) Chu, L.; Anastasio, C. *J. Phys. Chem. A* **2005**, *109*, 6264.

JP804622Z